Supplementary Materials for "GREMI: an Explainable Framework for Enhanced Disease Prediction and Module Identification" by Hong Liang, Haoran Luo, Zhiling Sang, Miao Jia, Xiaohan Jiang, Zheng Wang, Shan Cong, Xiaohui Yao.

S1 Supplementary Methods

S1.1 Multi-omics datasets and preprocessing.

We conducted extensive experiments on eight public datasets: four benchmark datasets, three cancer in-house processed datasets, and one independent dataset for validation.

ROSMAP is used for classifying Alzheimer's Disease (AD) patients versus normal control (NC). LGG is used for grade classification in low-grade glioma (LGG). KIPAN is used for kidney cancer type classification. BRCA is used for PAM50 subtype classification in breast invasive carcinoma (BRCA). LUAD is used for lung adenocarcinoma subtype classification. THCA is used for thyroid cancer subtype classification. UCEC is used for grade classification in uterine corpus endometrial carcinoma.

The benchmark datasets were obtained from Wang et al.[1], where ROSMAP and BRCA were downloaded from `https://github.com/txWang/MOGONET`, and the LGG and KIPAN were directly acquired from the authors. Detailed information regarding data acquisition and preprocessing were available in Wang et al.[1]. In brief, features with no signal (mean = 0) and low variances (standard deviation = 0.1 for mRNA, 0.001 for DNA methylation, and 0 for miRNA) were filtered out from each dataset. In addition, ANOVA tests were performed to further preselect features, aiming to decrease the negative effects of redundant features. Finally, every feature was scaled to [0,1] through a linear transformation. We also investigated how varying the number of features influenced model predictions on LGG and KIPAN datasets. Specifically, for each omics type, we extracted the top 1,000 (if available) and top 200 features based on the ANOVA F-value for comparison.

Besides four benchmark datasets, we extended the comparison using three cancer datasets (LUAD, THCA, and UCEC) to further demonstrate the stability and robustness of GREMI. To be specific, we downloaded raw multi-omics data for each disease from The Cancer Genome Atlas (TCGA, `https://portal.gdc.cancer.gov/`). Subsequently, we performed preprocessing for each dataset following the below criteria: (1) filter out features with no signal (mean = 0); (2) filter out features with low variances (standard deviation = 0.1 for mRNA, 0.001 for DNA methylation, and 0 for miRNA); (3) keep features exhibiting significant differences between classes (ANOVA FDR $P < 0.05$); (4) select top 200 features (i.e., features with the largest ANOVA F-values) for each omics type; (5) scale each feature into [0,1] interval via linear transformations.

We used an independent Chinese cohort to validate the predictive power of identified biomarkers. In detail, raw omics and clinical data of glioma patients were downloaded from the Chinese Glioma Genome Atlas (CGGA, http://www.cgga.org.cn/), including mRNAseq (batch 1) for a total of 693 samples, methylation microarray data for 159 samples, miRNA microarray data for 198 samples. Preprocessing was conducted to retain only the samples diagnosed with grades 2 and 3. Given that few methylation biomarkers and miRNA biomarkers identified from GREMI were available in CGGA data, we only kept the mRNA data in the LGG-V dataset and evaluated the performance of five mRNA biomarkers for CGGA LGG grade 2 vs. grade 3 classification.

S1.2 MCTS-based module identification

Algorithm 1 MCTS-based module identification algorithm.

Input: GREMI prediction model $F(\cdot)$, input graph $\mathcal{G}$, number of MCTS iterations T, module size threshold $N_{\min}$, $\mathcal{G}(S_i)$ denotes the associated subgraph of tree node S_i.
Initialization: Initialize the root node S_0 as the input graph $\mathcal{G}$. Initialize each node-action pair (S_i, a_{ij}): visit count N, total reward W, normalized action value Q, and prediction score P to 0. Initialize the leaf set as $S = \phi$.
for $t = 1$ to T **do**
    Set current node $S_i = S_0$, current node $curPath = [S_0]$
    while $\mathcal{G}(S_i)$ has more nodes than $N_{\min}$ **do**
        for all possible pruning actions a of $\mathcal{G}(S_i)$ **do**
            Obtain child nodes S_{ij} and its subgraph $\mathcal{G}(S_{ij})$.
            Compute $P(S_i, a_{ij}) = \text{Score}(F(\cdot), \mathcal{G}, \mathcal{G}(S_{S_{ij}}))$.
        end for
        Select the child node S_{next} according to Eqs.(7, 8).
        Update current node $S_i = S_{\text{next}}$, $curPath = curPath + S_{\text{next}}$.
    end while
    $S = S \cup \{S_i\}$
    Update nodes in $curPath$ according to Eqs.(9, 10).
end for
Output: Set of subgraphs within S that meet the size criteria.

S1.3 Detailed architecture of multi-level GAT

Here we detail the architecture of multi-level GAT used in our study. The input graph $\mathcal{G}_0$ has a feature dimension of $n \times 1$, where n denotes the number of nodes and 1 is the number of features on each node. To generate higher-level node representations, we stacked two GAT layers. Specifically, the first GAT layer consists of a 4-head attention mechanism with an input dimension of 1 and an output dimension of 8 for each attention head. The second GAT lay comprises a 3-head attention mechanism, where each attention head has an input dimension of 32 (concatenated output from the first layer) and an output dimension of 16. Each of the outputs from the first and second GAT layers was further projected to a dimension of 1 using a fully connected layer. We concatenated the original input features with the projected outputs from the first and second GAT layers to obtain a multi-level representation of each node. Subsequently, we fed the multi-level node representations into a multi-layer perceptron (MLP) with four hidden layers (600, 256, 64, 32) to produce sample embeddings.

S1.4 Time complexity and scalability analyses

We analyzed the time complexity of the proposed model and discussed how it scales with the size of the graph. Given that MCTS is known to be computationally expensive, we specifically focused on the MCTS-based module identification in our analysis. Generally, the time complexity of applying MCTS in module identification is $O(T \cdot (k_1 + \cdots + k_l)) \cdot O(\mathrm{F}(\cdot))$, where T represents the number of iterations, k_i is the number of pruning actions during the i-th expansion, l indicates the depth of the tree (i.e., the number of expansions) of each iteration, and $O(\mathrm{F}(\cdot))$ denotes the computational cost of model inference on the expanded subgraphs. In practical applications, we have implemented several strategies to effectively reduce the actual computational complexity: 1) During T iterations, each candidate subgraph obtained through expansion is stored, evaluated using a scoring function, and assigned a unique key. This allows us to bypass initiating expansions from the root repeatedly, significantly enhancing efficiency; 2) In each expansion step, rather than exploring all possible pruning actions, we rank the nodes by degree from low to high and only consider the top $k = 20$ (if available; refer to[2]) low-degree nodes. In practice, the number of possible pruning actions dramatically decreases after the first one or two expansions; 3) The MCTS can be executed in parallel because the module exploration for each sample is independent.

Using the ROSMAP mRNA concentrated co-functional graph (with 77 nodes) as an example, when we set the module size as 2 and configure $T = 20$, the average number of possible pruning actions per expansion is 565.7 (i.e., mean($\sum_{i=1}^{l} k_i$) = 565.7), and the average tree depth is 34.8 (i.e., mean(l) = 34.8), the time cost for a single model inference is approximately 0.005 seconds on an RTX 3090 GPU with 24 GB memory. The average computational time per sample is 52.9 seconds, with a memory usage of 14.27 MB. We consider this time and resource cost acceptable for practical application.

We acknowledge that scalability is critical for applying MCTS to large-scale graphs. However, based on the existing evidence (see Figure S2 in[1]) and our experiments (see Table III), increasing the number of features–which corresponds to the number of graph nodes–does not necessarily enhance prediction performance. Instead, it can lead to diminished performance, primarily due to introducing more redundant information. Our results indicate that incorporating 200 features per omics yields the best performance across benchmark datasets, suggesting that constructing extensive graphs may not be necessary for practical implementations.

Despite these observations, we continued to examine the time costs associated with running MCTS on graphs of varying scales. With $T = 20$, the running time of MCTS on graphs with 200 nodes is 689.8 seconds (memory usage of 14.29 MB), and for graphs with 1,000 nodes, the time is 1639.1 seconds (memory usage of 73.09MB). Given that the samples can be processed in parallel, both the time and space costs are considered acceptable.

S2 Supplementary Results

S2.1 Robustness evaluation under different feature missing rates

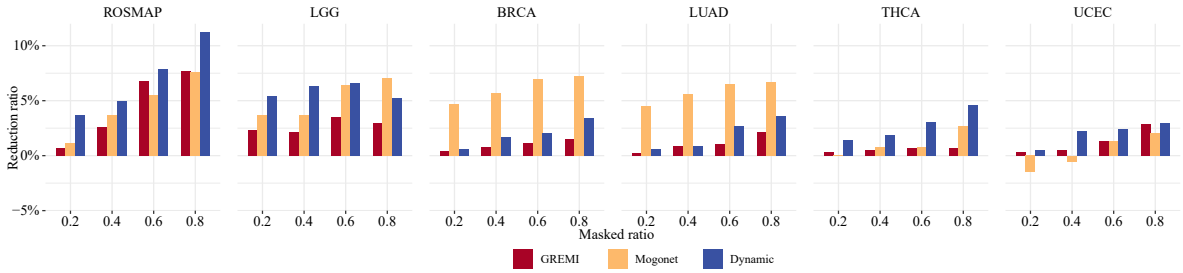

Figure S1: Robustness evaluation under different feature missing rates.

We assessed robustness against feature perturbation by setting varying feature missing rates (from 0.2 to 0.8) to the node and then compared the proposed model against others. We included the Mogonet and Dynamics in comparison, given their relatively good performances. Figure S1 illustrates the percentage decline in accuracy for each method at different missing rates. We can observe that our model consistently outperforms under various missing rates, exhibiting substantial robustness across lower and higher levels of perturbation in most of the datasets. This could be attributed to the graph-based modeling of molecule co-functional information and the confidence mechanism for trustworthy fusion.

S2.2 Robustness evaluation under different edge missing rates

We also explored the robustness of our proposed methods against perturbation in graph structure. We applied varying edge missing rates, ranging from 0.05 to 0.2, to each omics-specific network. Because other methods used the feature matrix (e.g., Dynamics) or sample-sample similarity network (e.g., Mogonet) as input, the edge perturbation cannot be directly applied to them. Therefore, we examined whether our method was affected by these graph structure perturbations. Figure S2 shows the results across six datasets, demonstrating that our model maintained stable performance across various levels of perturbations, with no significant decline in performance as the missing rate increased. These results suggest the efficiency of our model for real-world scenarios, which often include incomplete or highly noisy data.

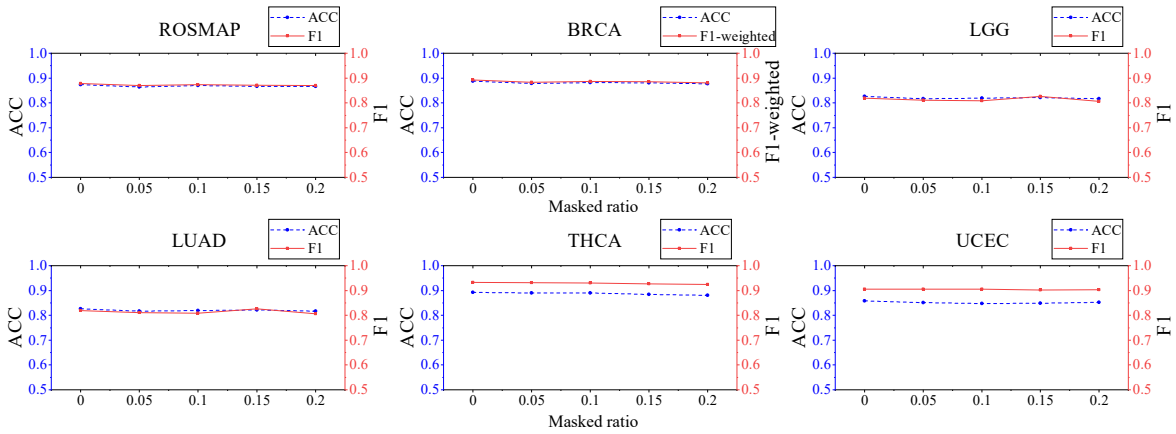

Figure S2: Robustness evaluation under different edge missing rates.

S2.3 Hyperparameter analysis

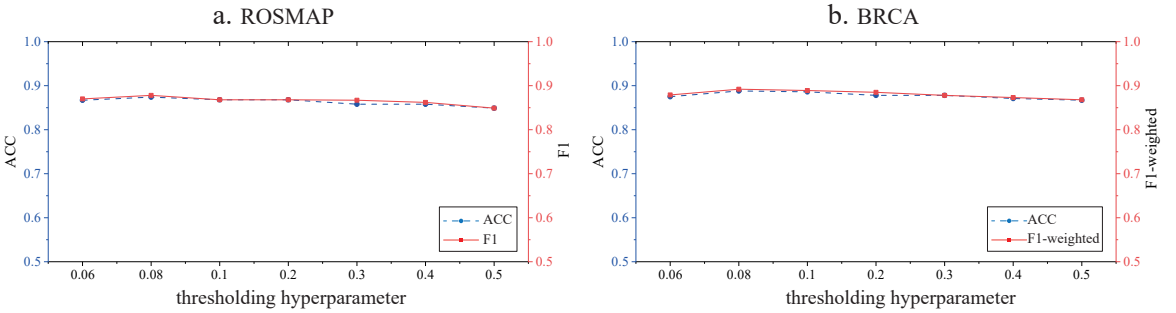

Figure S3: Performance metrics for ROSMAP and BRCA datasets across varying adjacency thresholds.

We evaluate the hyperparameter for thresholding the co-functional networks. This parameter was automatically tuned according to the classification accuracy within the range of [0.06, 0.08, 0.1, 0.2, 0.3, 0.4, 0.5]. For example, Figure S3(a,b) shows the grid search results, from which the optimal parameter 0.08 is selected for both ROSMAP and BRCA datasets. Furthermore, we can find that changing the threshold parameter had minimal impact on performance, demonstrating the robustness of the co-functional network structures for model performance.

S2.4 Module size setting and sensitivity analyses

In MCTS, the depth of the tree is influenced by the predefined module size; smaller module sizes typically result in deeper trees. In local-view module extraction, smaller modules are always nested within larger ones, motivating us to set small module sizes to facilitate the identification of more precise biomarkers. Although smaller module sizes are usually more time-consuming, the time required remains acceptable in practical applications, even when the module size is set to 2. For example, for a graph with 200 nodes, the average time for a module size of 2 is 689.8 seconds. Therefore, in implementation, we set the module sizes ranging from 2 to 5. Furthermore, the identified modules can be merged to construct large candidate sets, allowing us to explore a broader spectrum of potential targets, thereby expanding the utility and applicability of our findings in clinical settings.

Utilizing global-view results, we examined the proportion of smaller modules nested within larger modules. Taking results from ROSMAP mRNA as an example, we observed a significant overlap among modules of different sizes. Specifically, all size-2 modules were present in the size-3, size-4, and size-5 modules. Similarly, all of the size-3 modules were also present in both size-4 and size-5 modules. Furthermore, all size-4 modules were nested within size-5 modules. These findings suggest

that our method exhibits relatively low sensitivity to tree depth, enabling the robust identification of key biomarkers.

S2.5 Interpretation experiments

Within the supplementary results section, our investigation encompassed the application of the interpretation method to seven distinct diseases. Initially, we provided a concise overview of representative studies related to the individual-level biomarkers of AD and BRCA. Subsequently, we performed the interpretation method for five other diseases: LGG, KIPAN, LUAD, THCA, and UCEC. For each disease dataset, the interpretation method was applied to three distinct omics data types. In the ensuing discussion, we briefly analyzed the significant biomarkers from the various omics data for each disease, supported by an extensive literature review. For the significant modules, one module from each omics data was selected, and functional annotation for this module was conducted using both GO (Gene Ontology) and KEGG (Kyoto Encyclopedia of Genes and Genomes) databases[3]. The top ten significant pathways from GO and the top five significant pathways from KEGG of the selected module were then presented. Table S1 presents the details regarding the number of sample-wise important modules and consensus modules.

Table S1: Summary of the interpretations across seven diseases by GREMI.

Dataset	Omics type	The number of the consensus subgraphs
ROSMAP	mRNA	18
	methy	1
	miRNA	2
BRCA	mRNA	18
	methy	34
	miRNA	57
LGG	mRNA	18
	methy	18
	miRNA	26
KIPAN	mRNA	37
	methy	20
	miRNA	19
LUAD	mRNA	41
	methy	35
	miRNA	25
THCA	mRNA	30
	methy	41
	miRNA	26
UCEC	mRNA	19
	methy	6
	miRNA	4

S2.6 Top identified individual-level biomarkers of AD and BRCA.

Some of the top-identified individual biomarkers have shown relationships with AD and other neurodegenerative diseases. GWAS studies have reported the associations of *AC131056.3* and *MEIS3* with increased risk of AD[4,5]. In addition to AD, the *AC131056.3* has been identified to be associated with Parkinson's disease[6]. By integrating methylation and gene expression data from multiple brain regions, *ANKRD30B* exhibited differential methylation and differential expression between AD and controls[7]. Overexpression of miR-409-5p has been associated with impaired neurite outgrowth, reduced neuronal viability, and accelerated progression of $A\beta_{1-42}$-induced pathologies[8]. *HSPA6*, a member of the *HSP70* family, played a critical role in regulating protein misfolding, including tau levels and toxicity, within this pathological process associated with AD[9,10]. Physical activity has been shown to modulate miR-129-5p[11] and miR-132[12], both of which played important roles in alleviating cognitive impairment in AD and were considered to be potential therapeutic targets. Clinical studies have indicated that reduced levels of circulating miR-132 can function as a diagnostic biomarker for

AD[13]. Furthermore, its downregulation has been implicated in the pathogenesis of AD in both in vivo and in vitro models[14].

Table S2: Top identified individual-level biomarkers of AD and BRCA.

Dataset	Omics	Significant Biomarker
ROSMAP	mRNA	AC131056.3, ANKRD30B, DENND3-AS1, MEIS3, PPDPF
	methy	C1orf83, C10orf99, C19orf54, HSPA6, PLEK
	miRNA	hsa-miR-129-3p, hsa-miR-129-5p, hsa-miR-132, hsa-miR-133b
BRCA	mRNA	C1orf106, CHAC2, CPA4, CX3CL1, SFRP1
	methy	CLIC6, DCTN1, DNALI1, GPR37L1, IGFALS
	miRNA	hsa-mir-9-1, hsa-mir-187, hsa-mir-1301, hsa-mir-1304, hsa-mir-3934

The top individual biomarkers of BRCA also played important roles in the development and progression of various breast cancer subtypes. *C1orf106* has been recognized as a crucial regulator for basal-like/luminal progenitors and has been suggested for its potential as a therapeutic target for breast cancer[15]. A whole-transcriptome analysis has identified *CPA4* as a novel marker in breast cancer as well as a therapeutic target for triple-negative breast cancer (TNBC)[16]. *CLIC6*, a member of the chloride intracellular channel family, exhibited an altered expression profile in breast cancer[17]. A report suggested that polymorphisms in the *IGFBP3* genes may be linked to variations in survival outcomes among specific subgroups of breast cancer patients categorized by menopausal status[18]. Aberrant hypermethylation-induced epigenetic inactivation of the mir-9-1 gene was reported as a common and early event in breast cancer development[19]. By utilizing two independent cohorts, a breast cancer study[20] has indicated an association between high miR-187 expression and decreased breast cancer survival.

S2.7 GREMI identified biomarkers related to LGG.

Table S3 shows the top five significant biomarkers of each type of omics related to the LGG. Table S4 presents the significant modules of each type of omics related to the LGG. For mRNA modules, nine were identified, all of which had the same normalized impact. Each of these mRNA modules passed the permutation test. Modules with two features exhibited a P-value of 3E-2, those with three features had a P-value of 5E-3, and modules with four features showed a P-value less than 1E-3. For methylation modules, three were identified, each having the same normalized impact. All of these methylation co-function modules were found to be significant, with a P-value of 2E-3. Regarding miRNA co-function modules, two were identified, both of which were significant with a P-value of 3E-3.

Table S3: Important omics biomarkers identified by GREMI in the LGG dataset.

Omics	Significant Biomarker
mRNA	SFRP2, HMGCLL1, HPSE2, ALDOC, GLUD1
methy	LOC339568, AZGP1, C14orf68, C20orf71, C3orf27
miRNA	hsa-mir-491, hsa-mir-184, hsa-mir-383, hsa-mir-128-1, hsa-mir-1296

For significant biomarkers, secreted frizzled-related protein 2 (*SFRP2*) modulated Wnt signaling, acting either as an antagonist or agonist depending[21]. In mesenchymal stem cells, *SFRP2* overexpression diminished Wnt activity by reducing β-catenin levels[22]. *SFRP2* served as a tumor suppressor in various cancers, such as glioma, where its expression was reduced due to promoter hypermethylation[23]. *AZGP1*, showing significant amino-acid sequence similarity with tumor-derived lipid-mobilizing factor[24], was linked to cancer cachexia. In an AZGP1-producing tumor mouse model, it promoted adipocyte lipolysis, resulting in cachexia[25]. A result suggested that miR-491-5p and miR-491-3p played crucial roles as tumor suppressors in GBM, collectively targeting key oncogenes[26]. The miR-491-3p diminished glioma cell invasion, and the combined overexpression of both miRs impeded glioma cell proliferation and hinders glioma stem cell growth.

Table S4: Important omics modules identified by GREMI in the LGG dataset.

Omics	Significant Module
mRNA	[GSG2, MND1], [GSG2, MYBL2], [MND1, MYBL2], [GSG2, MND1, MYBL2], [DEPDC1B, GSG2, MYBL2], [DEPDC1B, MND1, MYBL2], [DEPDC1B, GSG2, MND1], [DEPDC1B, MCM2, MND1, MYBL2], [DEPDC1B, GSG2, MND1, MYBL2]
methy	[OR10X1, OR2A4], [MYO7B, OR10X1], [MYO7B, OR2A4],
miRNA	[hsa-mir-491, hsa-mir-495]

We performed functional annotations to the mRNA module [*DEPDC1B, MCM2, MND1, MYBL2*] and the methylation module [*OR10X1, OR2A4*]. Table S5 and Table S6 show the functional annotation results of the mRNA and methylation modules, respectively. Among the significant pathways presented in these tables, there were several pathways associated with the regulation of cell cycle, including GO:0090068 (P = 3.48E-2), GO:0045787 (P = 4.05E-2), and hsa04110 (P = 3.71E-2). TUBA1C, a subtype of α-tubulin, has been associated with the cell cycle pathways. It plays a crucial role in cellular mitosis and division[27]. Elevated expression of TUBA1C in LGG has been linked to a poor prognosis, suggesting its potential influence on tumor growth by modulating the tumor microenvironment[28]. For the methylation module, olfactory transduction was also identified in a previous study on glioblastoma[29]. In adult infiltrating glioma and GBM, losses at 9p21 were common[30–32]. Such deletions often resulted in the absence of the tumor suppressor CDKN2A[33]. Deletions in CDKN2A often coincided with BRAF p.V600E mutations, indicating its potential role as a molecular event that facilitates escaping from cell cycle regulation[34–36]. The above research findings directly or potentially confirmed the association between the modules and LGG.

Table S5: Significant pathways of the mRNA module of LGG.

Database	ID	Description	P.adjust
GO	GO:0006310	DNA recombination	3.56E-02
	GO:0000727	double-strand break repair via break-induced replication	3.56E-02
	GO:0051095	regulation of helicase activity	3.56E-02
	GO:1902969	mitotic DNA replication	3.56E-02
	GO:0000280	nuclear division	3.56E-02
	GO:0048285	organelle fission	3.56E-02
	GO:0006268	DNA unwinding involved in DNA replication	3.56E-02
	GO:0032780	negative regulation of ATPase activity	3.56E-02
	GO:0071353	cellular response to interleukin-4	4.10E-02
	GO:0070670	response to interleukin-4	4.10E-02
KEGG	hsa03030	DNA replication	8.56E-03
	hsa04218	Cellular senescence	3.68E-02
	hsa04110	Cell cycle	3.71E-02

Table S6: Significant pathways of the methylation module of LGG.

Database	ID	Description	P.adjust
GO	GO:0050911	detection of chemical stimulus involved in sensory perception of smell	2.58E-03
	GO:0007608	sensory perception of smell	2.58E-03
	GO:0050907	detection of chemical stimulus involved in sensory perception	2.58E-03
	GO:0032467	positive regulation of cytokinesis	1.34E-02
	GO:0051781	positive regulation of cell division	1.93E-02
	GO:0032465	regulation of cytokinesis	1.93E-02
	GO:0000910	cytokinesis	2.95E-02
	GO:0051302	regulation of cell division	2.95E-02
	GO:0090068	positive regulation of cell cycle process	3.48E-02
	GO:0045787	positive regulation of cell cycle	4.05E-02
KEGG	hsa04740	Olfactory transduction	2.73E-03

S2.8 GREMI identified biomarkers related to KIPAN.

Table S7 shows the top five significant biomarkers of each type of omics related to the KIPAN. As shown in Table S8, all mRNA modules were found to be significant with a P-value of 2E-3. The methylation co-function modules were also significant, exhibiting a P-value of 6E-3. Both identified miRNA co-function modules were significant with a P-value of 2E-2.

Table S7: Important omics biomarkers identified by GREMI in the KIPAN dataset.

Omics	Significant Biomarker
mRNA	AP1G2, C8orf74, COL4A4, EPHB2, ESPL1
methy	CRLF3, LOC145814, ABHD10, ACOT11, ADM
miRNA	hsa-mir-100, hsa-mir-126, hsa-mir-1271, hsa-mir-210, hsa-mir-424

In human cellular biology, two isoforms of the γ subunit were identified: *AP1G1* and *AP1G2*, sharing approximately 60% sequence identity. Downregulation of *AP1G1* has been observed in renal cancer tissues, correlating with reduced cell proliferation and migration[37]. It has been postulated that *AP1G2* may similarly exert influence on renal cancer pathogenesis[38]. *ACOT11*, a critical enzyme in fatty acid metabolism, has been identified as a diagnostic marker for clear cell renal cell carcinoma (ccRCC)[39]. The ccRCC was characterized by significant metabolic reprogramming across several pathways[40]. A prior study highlighted the role of miR-100 as a crucial prognostic indicator in RCC due to the correlation of its overexpression with advanced tumor stages and adverse patient outcomes[41]. Recent findings indicated a downregulation of miR-100 and an upregulation of *NOX4* in RCC tissues and cell lines[42]. *NOX4* has been confirmed as a target of miR-100. Elevated levels of miR-100 may enhance autophagy and reduce RCC cell invasion and migration by targeting *NOX4*, leading to inactivation of the mTOR pathway.

Table S8: Important omics modules identified by GREMI in the KIPAN dataset.

Omics	Significant Module
mRNA	[C8orf74, MPV17L2], [COL4A4, MPV17L2], [EPHB2, MPV17L2], [GYG2, MYB]
methy	[C19orf26, COBRA1], [C18orf54, COBRA1]
miRNA	[hsa-mir-126, hsa-mir-143], [hsa-mir-126, hsa-mir-497]

Functional annotations were conducted to the mRNA module containing [*C8orf74, MPV17L2*] and the methylation module containing [*C19orf26, COBRA1*]. Table S9 presents the functional annotation results for the mRNA module. However, the functional annotation for the methylation module

was not found to be significant. As illustrated in Table S9, several pathways associated with mitochondrial processes were identified, including GO:0061668 (P = 4.84E-3), GO:0070131 (P = 4.84E-3), GO:0070129 (P = 4.84E-3), GO:0062125 (P = 4.84E-3), and so on. Mitochondria played a central role in cellular energy generation via oxidative phosphorylation to regulate calcium balance, and were crucial in the processes of apoptosis[43]. The mitochondrial respiratory system was the chief intracellular contributor of reactive oxygen species (ROS), pivotal for maintaining redox stability and cellular signal transduction[44]. Marquardt et al.[45] identified a unique histopathological subgroup in RCC using RNA-sequencing analysis. This subgroup markedly impacted the survival rates, decreasing them in ccRCC patients and increasing them in chRCC patients. In contrast, a majority of oncocytomas had malfunctioning mitochondria attributed to mutations in the first complex and obstructed mitochondrial clearance mechanisms[46,47]. Additionally, mutations in metabolic enzymes, notably fumarate hydratase (FH) and succinate dehydrogenase (SDH), underpinned the onset of FH-deficient RCC[48] and SDH-deficient RCC[49].

Table S9: Significant pathways of the mRNA module of KIPAN.

Database	ID	Description	P.adjust
GO	GO:0061668	mitochondrial ribosome assembly	4.84E-03
	GO:0070131	positive regulation of mitochondrial translation	4.84E-03
	GO:0070129	regulation of mitochondrial translation	4.84E-03
	GO:0062125	regulation of mitochondrial gene expression	4.84E-03
	GO:0042255	ribosome assembly	8.30E-03
	GO:0032543	mitochondrial translation	8.30E-03
	GO:0140053	mitochondrial gene expression	1.03E-02
	GO:0045727	positive regulation of translation	1.22E-02
	GO:0034250	positive regulation of cellular amide metabolic process	1.28E-02
	GO:0042254	ribosome biogenesis	2.10E-02
KEGG	hsa04146	Peroxisome	9.77E-03

S2.9 GREMI identified biomarkers related to LUAD.

Table S10 shows the top five significant biomarkers of each type of omics related to the LUAD. As detailed in Table S11, all 23 genetic factors within the mRNA modules exhibited significance with a P-value of 2E-3. Furthermore, all eight methylation co-function modules and all five miRNA co-function modules demonstrated high significance, each with a P-value less than 1E-3.

Table S10: Important omics biomarkers identified by GREMI in the LUAD dataset.

Omics	Significant Biomarker
mRNA	PRKAR1A, SLC24A1, CRB3, GPR20, HFE
methy	A2ML1, AADACL3, AADACL4, ABAT, ABCC11
miRNA	hsa-mir-1250, hsa-mir-1266, hsa-mir-129-1, hsa-mir-129-2, hsa-mir-3609

Significant biomarkers play crucial roles in understanding disease progression and therapeutic responses. Among these, Protein Kinase cAMP-Dependent Regulatory Type I Alpha (*PRKAR1A*) functioned as a tissue-specific modulator, exerting its effects through the phosphorylation of various target proteins[50].*PRKAR1A* deficiency has been identified in endocrine neoplasia and stromal cell tumors. Recent investigations have revealed a significant downregulation of *PRKAR1A* in patients with lung adenocarcinoma[51]. This reduced expression of *PRKAR1A* was associated with advanced tumor stages and diminished overall survival rates. Furthermore, reintroducing *PRKAR1A* in H1299 cell lines led to a marked decrease in both tumor cell proliferation and migration. Thus, *PRKAR1A* emerged as a critical suppressor, and targeting the PRKAR1A-ERK-Snail-E-cadherin pathway may offer therapeutic potential. *A2ML1*, a protease inhibitor, was a member of the alpha-macroglobulin superfamily[52,53]. This inhibitor exhibited a distinct trap mechanism, wherein a significant conformational shift occurred in *A2ML1* upon protease cleavage, effectively ensnaring the protease and preventing further substrate binding. Recent research has highlighted a correlation between the methylation of TRIM58 and the treatment of lung squamous cell carcinoma, with *A2ML1* being identified as a potential prognostic biomarker[54]. In the LUAD, methylation-mediated silencing has been observed to influence miR-1250-5p, leading to the upregulation of its direct target, WDR1[55]. Previous study observed an elevated expression of WDR1 in lung cancer, with a correlation to unfavorable prognosis[56]. In lung cancer cells, the oncogenic role of WDR1 manifested in its ability to modulate cellular proliferation. This modulation occured through dephosphorylation, enhancing the nuclear translocation of the YAP protein. The YAP protein was a key effector in the Hippo signaling pathway, which in turn activated genes that promoted cell proliferation.

Table S11: Important omics modules identified by GREMI in the LUAD dataset.

Omics	Significant Module
mRNA	[PLK1, TPX2], [PLK1, RAD54L], [RAD54L, TPX2], [CDCA5, PLK1], [KIF18B, PLK1], [CDCA5, TPX2], [KIF18B, TPX2], [CDCA5, RAD54L], [KIF18B, RAD54L], [KIF4A, TPX2], [KIF4A, PLK1], [CENPE, PLK1], [CENPE, TPX2], [KIF4A, RAD54L], [CENPE, RAD54L], [CDCA5, KIF18B], [CDCA5, PKMYT1], [KIF18B, PKMYT1], [CDCA5, KIF4A], [CDCA5, CENPE], [KIF18B, KIF4A], [CENPE, KIF18B], [CENPE, KIF4A]
methy	[C10orf120, CST4], [CST4, DCLK3], [C10orf120, CRTAM], [CST4, FOLR4], [CRTAM, CST4], [CST1, CST4], [AQP10, CST4], [CRTAM, CST1]
miRNA	[hsa-let-7a-2, hsa-let-7f-2], [hsa-let-7a-2, hsa-let-7a-3], [hsa-let-7a-1, hsa-let-7a-2], [hsa-let-7a-1, hsa-let-7a-3], [hsa-let-7a-3, hsa-let-7f-2]

We performed functional annotations to the mRNA module [*PLK1, TPX2*] and the methylation module [*C10orf120, CST4*]. Table S12 and Table S13 show the functional annotation results of the mRNA and methylation modules, respectively. As shown in Table S12, there were several enriched pathways associated with mitotic spindle, including GO:0060236 (P = 4.91E-4), GO:0090224 (P = 4.91E-4), GO:0090307 (P = 8.50E-4), GO:0051225 (P = 1.66E-3), GO:0007052 (P = = 1.66E-3), and so on. Chronic obstructive lung disease (COPD) was a persistent pulmonary condition, with

50%-80% of lung cancer patients exhibiting preexisting COPD[57]. 4-(methylnitrosamino)-1-(3-pyridyl)-1-butanone (NNK) contributed to tumor initiation by forming DNA adducts, leading to mutations in oncogenes and tumor suppressor genes[58]. Crucially, disruptions in the mitotic spindle apparatus significantly influenced genomic instability, primarily by facilitating chromosome mis-segregation and aneuploidy[59]. Recent studies indicated that NNK exacerbated chromosomal instability by interfering with spindle microtubule attachment to the kinetochore and altering spindle dynamics[60]. As for the hsa04068 (P = 1.87E-2), Forkhead box O (FOXO) transcription factored orchestrate many cellular processes including development, metabolism, and stem cell homeostasis[61]. Their pivotal role in tumorigenesis was highlighted by the capacity of modulating gene expression. Specifically, the metastasis suppressor gene nm23-H1, implicated in attenuating the progression of malignancies such as non-small cell lung cancer (NSCLC), was positively regulated by FOXO1 in pulmonary neoplasms[62]. FOXO3 has been identified as a significant factor in the metastasis of many malignancies[63,64]. In addition, many pathways of the methylation module presented association with the sensory perception of taste. In a systematic scoping review on lung cancer[65], a noted prevalence ranged from 12% to 84% for self-reported taste disturbances among oncology patients[66]. A single-center study with 239 diverse cancer patients, including nine with lung cancer, indicated dysphagia in 54%, taste alterations in 62%, and olfactory changes in 35%[67]. The research results discussed above directly or potentially confirmed the relation between the modules and LUAD.

Table S12: Significant pathways of the mRNA module of LUAD.

Database	ID	Description	P.adjust
GO	GO:0060236	regulation of mitotic spindle organization	4.91E-04
	GO:0090224	regulation of spindle organization	4.91E-04
	GO:0090307	mitotic spindle assembly	8.50E-04
	GO:0051225	spindle assembly	1.66E-03
	GO:0007052	mitotic spindle organization	1.66E-03
	GO:1902850	microtubule cytoskeleton organization involved in mitosis	1.78E-03
	GO:0070507	regulation of microtubule cytoskeleton organization	1.78E-03
	GO:0007051	spindle organization	2.39E-03
	GO:0032886	regulation of microtubule-based process	3.73E-03
	GO:0140014	mitotic nuclear division	4.65E-03
KEGG	hsa04914	Progesterone-mediated oocyte maturation	1.87E-02
	hsa04068	FoxO signaling pathway	1.87E-02
	hsa04114	Oocyte meiosis	1.87E-02
	hsa04110	Cell cycle	1.87E-02

Table S13: Significant pathways of the methylation module of LUAD.

Database	ID	Description	P.adjust
GO	GO:0001580	detection of chemical stimulus involved in sensory perception of bitter taste	1.07E-02
	GO:0050913	sensory perception of bitter taste	1.07E-02
	GO:0050912	detection of chemical stimulus involved in sensory perception of taste	1.07E-02
	GO:0050909	sensory perception of taste	1.17E-02
	GO:0001895	retina homeostasis	1.19E-02
	GO:0010951	negative regulation of endopeptidase activity	2.51E-02
	GO:0010466	negative regulation of peptidase activity	2.51E-02
	GO:0001894	tissue homeostasis	2.51E-02
	GO:0060249	anatomical structure homeostasis	2.51E-02
	GO:0045861	negative regulation of proteolysis	2.51E-02
KEGG	hsa04970	Salivary secretion	1.11E-02

S2.10 GREMI identified biomarkers related to THCA.

Table S14 shows the top five significant biomarkers of each type of omics related to the THCA. As detailed in Table S15, both mRNA modules exhibited significance with a P-value of 2E-3. All five methylation co-function modules demonstrated high significance with a P-value less than 1E-3. Additionally, the miRNA co-function module was significant with a P-value of 2E-2.

For significant biomarkers, *FAM155B* stood out as a pivotal gene related to the B-type Raf (BRAF) kinase mutation in papillary thyroid cancer. Its expression varied significantly between the wild-type and its mutant counterpart[68]. In addition, Choi et al. formulated a 12-genes predictive model, with *FAM155B* being a key component, leveraging data from the TCGA THCA dataset to potentially forecast nodal metastasis in PTC[69]. Researchers have discovered an elevated expression of *GPR115* in thyroid carcinoma, with its methylation playing a significant role in lung cancer therapy[70]. This suggested that *GPR115* could be instrumental in driving tumor growth. Additionally, a study highlighted the potential of *GPR115* as a connecting factor between tumor advancement and survival prognosis, positioning it as a potential biomarker for LUAD treatment[71]. A study revealed that miR-618 was downregulated in thyroid cancer (TC)[72]. This downregulation was associated with a growth-suppressive effect in TC cells, largely attributed to its targeting of the PI3K/Akt signaling pathway. This finding emphasized the profound connection between miR-618 and TC.

Table S14: Important omics biomarkers identified by GREMI in the THCA dataset.

Omics	Significant Biomarker
mRNA	FAM155B, ABHD10, BCAP29, BTBD11, LOC286002
methy	C1orf180, CAPG, GPR115, KLF6, KRT13
miRNA	hsa-mir-618, hsa-mir-1179, hsa-mir-144, hsa-mir-185, hsa-mir-190

Table S15: Important omics modules identified by GREMI in the THCA dataset.

Omics	Significant Module
mRNA	[BTBD11, CYB5D1, GNA14], [ANKRD46, BTBD11, GNA14]
methy	[GPR115, MMP7], [KLF6, MMP7], [MMP7, SNHG3], [GPR115, KRT13], [CAPG, MMP7]
miRNA	[hsa-mir-1179, hsa-mir-7-2]

We performed functional annotations to the mRNA module [*BTBD11, CYB5D1, GNA14*] and the methylation module [*GPR115, MMP7*]. Table S16 and Table S17 show the annotation results of the mRNA and methylation modules, respectively. SMAD protein signal transduction (GO:0060395, P = 1.65E-2) was integral to SMAD family cellular processes, with SMAD3 being a central signaling molecule in the transforming growth factor-β (TGF-β) pathway. This molecule has been implicated in apoptosis, metastasis, and tumor progression[73,74]. A recent study indicated the role of SMAD3 in regulating SPRY4 and SPRY4-IT1 as a transcriptional factor, suggesting its potential association with thyroid cancer predisposition[75]. In addition, calcium signaling pathway (hsa04020, P = 2.86E-2) presented to be highly associated with thyroid cancer. A review highlighted the pivotal role of calcium pathways in thyroid function[76]. For example, proteins of the S100A category was related to multiple malignancies[77], including thyroid tumors. Specifically, proteins like S100A13[78] and S100A4[79] were instrumental in influencing the growth, infiltration, and spread of thyroid carcinoma cells. For the methylation module, Wnt signaling pathway (hsa04310, P = 2.65E-2) was significant. A previous review[80] highlighted the role of Wnt signaling in thyroid physiology, including its development, equilibrium, and tumorigenesis[81]. Individuals with Familial Adenomatous Polyposis (FAP), Gardner's syndrome, or Turcot's syndrome possessing APC gene mutations exhibited heightened thyroid cancer susceptibility due to aberrant Wnt signaling[82,83]. Furthermore, Wnt signaling has been identified as a regulatory factor in Follicular thyroid carcinoma (FTC)[84]. Anaplastic thyroid carcinomas (ATC), recognized as highly aggressive malignancies, frequently exhibited reduced Wnt-5a expression, which was associated with enhanced malignancy[85]. The aforementioned research conclusions directly or potentially confirmed the association between the modules and THCA.

Table S16: Significant pathways of the mRNA module of THCA.

Database	ID	Description	P.adjust
GO	GO:0007212	dopamine receptor signaling pathway	1.65E-02
	GO:0060395	SMAD protein signal transduction	1.65E-02
	GO:1903351	cellular response to dopamine	1.65E-02
	GO:1903350	response to dopamine	1.65E-02
	GO:0007200	phospholipase C-activating G protein-coupled receptor signaling pathway	1.65E-02
	GO:0071868	cellular response to monoamine stimulus	1.65E-02
	GO:0071870	cellular response to catecholamine stimulus	1.65E-02
	GO:0071867	response to monoamine	1.65E-02
	GO:0071869	response to catecholamine	1.65E-02
	GO:0001508	action potential	1.97E-02
KEGG	hsa05142	Chagas disease	1.82E-02
	hsa05146	Amoebiasis	1.82E-02
	hsa04020	Calcium signaling pathway	2.86E-02

Table S17: Significant pathways of the methylation module of THCA.

Database	ID	Description	P.adjust
GO	GO:0031293	membrane protein intracellular domain proteolysis	5.85E-03
	GO:0030574	collagen catabolic process	6.60E-03
	GO:0006509	membrane protein ectodomain proteolysis	6.60E-03
	GO:0033619	membrane protein proteolysis	6.60E-03
	GO:0022617	extracellular matrix disassembly	6.60E-03
	GO:0032963	collagen metabolic process	8.95E-03
	GO:0030198	extracellular matrix organization	1.83E-02
	GO:0043062	extracellular structure organization	1.83E-02
	GO:0045229	external encapsulating structure organization	1.83E-02
	GO:0022411	cellular component disassembly	2.45E-02
KEGG	hsa04310	Wnt signaling pathway	2.65E-02
	hsa05166	Human T-cell leukemia virus 1 infection	2.65E-02

S2.11 GREMI identified biomarkers related to UCEC.

Table S18 shows the top five significant biomarkers of each type of omics related to the UCEC. As illustrated in Table S19, the mRNA co-function module exhibited significance with a P-value of 3E-2. The methylation co-function module demonstrated high significance, with a P-value less than 1E-3. All three miRNA co-function modules were significant, each with a P-value of 2E-2).

Table S18: Important omics biomarkers identified by GREMI in the UCEC dataset.

Omics	Significant Biomarker
mRNA	AACS, C16orf89, ANKLE2, PIAS3, RICH2
methy	CAMK2N1, PPP1R15A, C5orf62, LTBP3, SAP30BP
miRNA	hsa-mir-664, hsa-mir-20b, hsa-mir-144, hsa-mir-27a, hsa-mir-508

As for the significant biomarkers, endometrial cancer (EC) was the leading gynecologic malignancy in the US. A study revealed that the tumor suppressor gene *PIAS3* showed decreased expression in adipose and uterine tissues, revealing the mechanism of obesity-induced TMEM205 expression and exosome secretion in the pathogenesis of EC[86]. *PPP1R15A*, also termed *GADD34*, was a stress-responsive eIF2α phosphatase that could enhance cell death through increased protein synthesis and activation of death-associated pathways[87]. A recent study identified *PPP1R15A* as an ER stress-associated risk signature for predicting the prognosis of EC patients[88]. In addition, a study on MicroRNA signatures identified distinct patterns among uterine cancer tumor subtypes[89]. Specifically, carcinosarcomas showed a unique miRNA profile with an up-regulation of miR-20b.

Table S19: Important omics modules identified by GREMI in the UCEC dataset.

Omics	Significant Module
mRNA	[SRPRB, WASF3]
methy	[APOL3, RCC1]
miRNA	[hsa-let-7i, hsa-mir-103-1], [hsa-mir-100, hsa-mir-103-1], [hsa-let-7i, hsa-mir-100]

We performed functional annotations to the mRNA module [*SRPRB, WASF3*] and the methylation module [*APOL3, RCC1*]. Table S20 and Table S21 show the annotation results of the mRNA and methylation modules, respectively. For the mRNA module, there were several pathways associated with the regulation of actin nucleation, including GO:2000601 (P = 1.52E-2), GO:0051127 (P = 1.52E-2), GO:0034315 (P = 1.57E-2), and GO:0051125 (P = 1.60E-2). Arp2/3 complex-mediated actin nucleation (GO:2000601) was significantly influenced by ARPC5, which is a core component of the complex[90]. Deviations in ARPC5 expression can potentially affect the entire function of the complex. Multiple research findings have indicated that ARPC5 promotes tumor expansion and metastasis.[91,92]. Choline metabolism was also enriched. A research[93] suggested that EC exhibited disrupted choline phospholipid metabolism due to heightened expression of choline kinase alpha and an intensified deacylation pathway. This cancer presented marked lipid metabolism anomalies, with elevated phosphocholine levels as the primary lipid alteration. For the methylation module, both GO:0051225 and GO:0007052 were related to the organization and assembly of the spindle. Correct mitotic spindle orientation during cell division was crucial for determining cell fate, orchestrating tissue structure, and guiding development. Alterations in microtubule dynamics affecting the mitotic spindle can cause chromosomal instability, subsequently resulting in the production of tumorigenic cells[94,95]. Li et al. also identified the mitotic spindle from the result of gene set enrichment analysis[96]. They found that mitotic spindles played roles in DNA damage repair and cell cycle control. Disruptions in these pathways frequently correlated with tumor initiation and advancement. Previous research findings directly or potentially confirmed the association between the modules and UCEC.

Table S20: Significant pathways of the mRNA module of UCEC.

Database	ID	Description	P.adjust
GO	GO:0098885	modification of postsynaptic actin cytoskeleton	1.52E-02
	GO:2000601	positive regulation of Arp2/3 complex-mediated actin nucleation	1.52E-02
	GO:0099010	modification of postsynaptic structure	1.52E-02
	GO:0051127	positive regulation of actin nucleation	1.52E-02
	GO:0031643	positive regulation of myelination	1.52E-02
	GO:0099563	modification of synaptic structure	1.52E-02
	GO:0034315	regulation of Arp2/3 complex-mediated actin nucleation	1.57E-02
	GO:0051125	regulation of actin nucleation	1.60E-02
	GO:0031646	positive regulation of nervous system process	1.60E-02
	GO:0014003	oligodendrocyte development	1.60E-02
KEGG	hsa03060	Protein export	3.29E-02
	hsa04520	Adherens junction	3.48E-02
	hsa04666	Fc gamma R-mediated phagocytosis	3.48E-02
	hsa05231	Choline metabolism in cancer	3.48E-02

Table S21: Significant pathways of the methylation module of UCEC.

Database	ID	Description	P.adjust
GO	GO:0007084	mitotic nuclear membrane reassembly	1.44E-02
	GO:0101024	mitotic nuclear membrane organization	1.44E-02
	GO:0031468	nuclear membrane reassembly	2.45E-02
	GO:0071763	nuclear membrane organization	2.82E-02
	GO:0006998	nuclear envelope organization	2.82E-02
	GO:0071709	membrane assembly	2.82E-02
	GO:0044091	membrane biogenesis	2.82E-02
	GO:0007088	regulation of mitotic nuclear division	3.42E-02
	GO:0051225	spindle assembly	3.42E-02
	GO:0007052	mitotic spindle organization	3.42E-02

References

[1] T. Wang, W. Shao, Z. Huang, H. Tang, J. Zhang, Z. Ding, and K. Huang, "Mogonet integrates multi-omics data using graph convolutional networks allowing patient classification and biomarker identification," *Nature Communications*, vol. 12, no. 1, pp. 1–13, 2021.

[2] H. Yuan, H. Yu, J. Wang, K. Li, and S. Ji, "On explainability of graph neural networks via subgraph explorations," in *Proceedings of the 38th International Conference on Machine Learning* (M. Meila and T. Zhang, eds.), vol. 139 of *Proceedings of Machine Learning Research*, pp. 12241–12252, PMLR, 18–24 Jul 2021.

[3] T. Wu, E. Hu, S. Xu, M. Chen, P. Guo, Z. Dai, T. Feng, L. Zhou, W. Tang, L. Zhan, *et al.*, "clusterprofiler 4.0: A universal enrichment tool for interpreting omics data," *The Innovation*, vol. 2, no. 3, p. 100141, 2021.

[4] C. Bellenguez, F. Küçükali, I. E. Jansen, L. Kleineidam, S. Moreno-Grau, N. Amin, A. C. Naj, R. Campos-Martin, B. Grenier-Boley, V. Andrade, *et al.*, "New insights into the genetic etiology of alzheimer's disease and related dementias," *Nature genetics*, vol. 54, no. 4, pp. 412–436, 2022.

[5] B. W. Kunkle, B. Grenier-Boley, R. Sims, J. C. Bis, V. Damotte, A. C. Naj, A. Boland, M. Vronskaya, S. J. Van Der Lee, A. Amlie-Wolf, *et al.*, "Genetic meta-analysis of diagnosed alzheimer's disease identifies new risk loci and implicates aβ, tau, immunity and lipid processing," *Nature genetics*, vol. 51, no. 3, pp. 414–430, 2019.

[6] Y. Fan, J. Li, Q. Yang, C. Gong, H. Gao, Z. Mao, X. Yuan, S. Zhu, and Z. Xue, "Dysregulated long non-coding rnas in parkinson's disease contribute to the apoptosis of human neuroblastoma cells," *Frontiers in Neuroscience*, vol. 13, p. 1320, 2019.

[7] S. A. Semick, R. A. Bharadwaj, L. Collado-Torres, R. Tao, J. H. Shin, A. Deep-Soboslay, J. R. Weiss, D. R. Weinberger, T. M. Hyde, J. E. Kleinman, *et al.*, "Integrated dna methylation and gene expression profiling across multiple brain regions implicate novel genes in alzheimer's disease," *Acta neuropathologica*, vol. 137, pp. 557–569, 2019.

[8] J. Guo, Y. Cai, X. Ye, N. Ma, Y. Wang, B. Yu, and J. Wan, "Mir-409-5p as a regulator of neurite growth is down regulated in app/ps1 murine model of alzheimer's disease," *Frontiers in Neuroscience*, vol. 13, p. 1264, 2019.

[9] B. Bukau, J. Weissman, and A. Horwich, "Molecular chaperones and protein quality control," *Cell*, vol. 125, no. 3, pp. 443–451, 2006.

[10] R. E. Lackie, A. Maciejewski, V. G. Ostapchenko, J. Marques-Lopes, W.-Y. Choy, M. L. Duennwald, V. F. Prado, and M. A. Prado, "The hsp70/hsp90 chaperone machinery in neurodegenerative diseases," *Frontiers in neuroscience*, vol. 11, p. 254, 2017.

[11] Z. Li, Q. Chen, J. Liu, and Y. Du, "Physical exercise ameliorates the cognitive function and attenuates the neuroinflammation of alzheimer's disease via mir-129–5p," *Dementia and geriatric cognitive disorders*, vol. 49, no. 2, pp. 163–169, 2020.

[12] J. Dong, Y. Liu, Z. Zhan, and X. Wang, "Microrna-132 is associated with the cognition improvement following voluntary exercise in samp8 mice," *Brain research bulletin*, vol. 140, pp. 80–87, 2018.

[13] M. Zhang and Z. Bian, "Alzheimer's disease and microrna-132: a widespread pathological factor and potential therapeutic target," *Frontiers in Neuroscience*, vol. 15, p. 687973, 2021.

[14] R. El Fatimy, S. Li, Z. Chen, T. Mushannen, S. Gongala, Z. Wei, D. T. Balu, R. Rabinovsky, A. Cantlon, A. Elkhal, *et al.*, "Microrna-132 provides neuroprotection for tauopathies via multiple signaling pathways," *Acta Neuropathologica*, vol. 136, pp. 537–555, 2018.

[15] J. Ma, C. Liu, D. Yang, J. Song, J. Zhang, T. Wang, M. Wang, W. Xu, X. Li, S. Ding, *et al.*, "C1orf106, an innate immunity activator, is amplified in breast cancer and is required for basal-like/luminal progenitor fate decision," *Science China Life Sciences*, vol. 62, pp. 1229–1242, 2019.

[16] T. Handa, A. Katayama, T. Yokobori, A. Yamane, T. Fujii, S. Obayashi, S. Kurozumi, R. Kawabata-Iwakawa, N. Gombodorj, M. Nishiyama, *et al.*, "Carboxypeptidase a4 accumulation is associated with an aggressive phenotype and poor prognosis in triple-negative breast cancer," *International journal of oncology*, vol. 54, no. 3, pp. 833–844, 2019.

[17] J.-H. Ko, E. A. Ko, W. Gu, I. Lim, H. Bang, and T. Zhou, "Expression profiling of ion channel genes predicts clinical outcome in breast cancer," *Molecular cancer*, vol. 12, no. 1, pp. 1–17, 2013.

[18] S. L. Deming, Z. Ren, W. Wen, X. O. Shu, Q. Cai, Y.-T. Gao, and W. Zheng, "Genetic variation in igf1, igf-1r, igfals, and igfbp3 in breast cancer survival among chinese women: a report from the shanghai breast cancer study," *Breast cancer research and treatment*, vol. 104, pp. 309–319, 2007.

[19] U. Lehmann, B. Hasemeier, M. Christgen, M. Müller, D. Römermann, F. Länger, and H. Kreipe, "Epigenetic inactivation of microrna gene hsa-mir-9-1 in human breast cancer," *The Journal of Pathology: A Journal of the Pathological Society of Great Britain and Ireland*, vol. 214, no. 1, pp. 17–24, 2008.

[20] L. Mulrane, S. F. Madden, D. J. Brennan, G. Gremel, S. F. McGee, S. McNally, F. Martin, J. P. Crown, K. Jirström, D. G. Higgins, *et al.*, "mir-187 is an independent prognostic factor in breast cancer and confers increased invasive potential in vitromir-187 and breast cancer," *Clinical cancer research*, vol. 18, no. 24, pp. 6702–6713, 2012.

[21] K. van Loon, E. J. Huijbers, and A. W. Griffioen, "Secreted frizzled-related protein 2: a key player in noncanonical wnt signaling and tumor angiogenesis," *Cancer and Metastasis Reviews*, vol. 40, pp. 191–203, 2021.

[22] M. P. Alfaro, A. Vincent, S. Saraswati, C. A. Thorne, C. C. Hong, E. Lee, and P. P. Young, "sfrp2 suppression of bone morphogenic protein (bmp) and wnt signaling mediates mesenchymal stem cell (msc) self-renewal promoting engraftment and myocardial repair," *Journal of Biological Chemistry*, vol. 285, no. 46, pp. 35645–35653, 2010.

[23] S. Götze, M. Wolter, G. Reifenberger, O. Müller, and S. Sievers, "Frequent promoter hypermethylation of wnt pathway inhibitor genes in malignant astrocytic gliomas," *International journal of cancer*, vol. 126, no. 11, pp. 2584–2593, 2010.

[24] S. T. Russell, T. P. Zimmerman, B. A. Domin, and M. J. Tisdale, "Induction of lipolysis in vitro and loss of body fat in vivo by zinc-α2-glycoprotein," *Biochimica et Biophysica Acta (BBA)-Molecular and Cell Biology of Lipids*, vol. 1636, no. 1, pp. 59–68, 2004.

[25] C. Bing, Y. Bao, J. Jenkins, P. Sanders, M. Manieri, S. Cinti, M. J. Tisdale, and P. Trayhurn, "Zinc-α2-glycoprotein, a lipid mobilizing factor, is expressed in adipocytes and is up-regulated in mice with cancer cachexia," *Proceedings of the National Academy of Sciences*, vol. 101, no. 8, pp. 2500–2505, 2004.

[26] X. Li, Y. Liu, K. J. Granberg, Q. Wang, L. M. Moore, P. Ji, J. Gumin, E. P. Sulman, G. A. Calin, H. Haapasalo, *et al.*, "Two mature products of mir-491 coordinate to suppress key cancer hallmarks in glioblastoma," *Oncogene*, vol. 34, no. 13, pp. 1619–1628, 2015.

[27] M. A. H. Albahde, P. Zhang, Q. Zhang, G. Li, and W. Wang, "Upregulated expression of tuba1c predicts poor prognosis and promotes oncogenesis in pancreatic ductal adenocarcinoma via regulating the cell cycle," *Frontiers in oncology*, vol. 10, p. 49, 2020.

[28] H. Zhu, X. Hu, L. Gu, Z. Jian, L. Li, S. Hu, S. Qiu, and X. Xiong, "Tuba1c is a prognostic marker in low-grade glioma and correlates with immune cell infiltration in the tumor microenvironment," *Frontiers in Genetics*, vol. 12, p. 759953, 2021.

[29] L. Zhou, H. Tang, F. Wang, L. Chen, S. Ou, T. Wu, J. Xu, and K. Guo, "Bioinformatics analyses of significant genes, related pathways and candidate prognostic biomarkers in glioblastoma," *Molecular medicine reports*, vol. 18, no. 5, pp. 4185–4196, 2018.

[30] W. Biernat, Y. Tohma, Y. Yonekawa, P. Kleihues, and H. Ohgaki, "Alterations of cell cycle regulatory genes in primary (de novo) and secondary glioblastomas," *Acta neuropathologica*, vol. 94, pp. 303–309, 1997.

[31] H. Ohgaki and P. Kleihues, "Genetic alterations and signaling pathways in the evolution of gliomas," *Cancer science*, vol. 100, no. 12, pp. 2235–2241, 2009.

[32] M. Pekmezci, M. Stevers, J. J. Phillips, J. Van Ziffle, B. C. Bastian, N. M. Tsankova, B. K. Kleinschmidt-DeMasters, M. K. Rosenblum, T. Tihan, A. Perry, *et al.*, "Multinodular and vacuolating neuronal tumor of the cerebrum is a clonal neoplasm defined by genetic alterations that activate the map kinase signaling pathway," *Acta neuropathologica*, vol. 135, pp. 485–488, 2018.

[33] M. Ruas and G. Peters, "The p16ink4a/cdkn2a tumor suppressor and its relatives.," *Biochimica et biophysica acta*, vol. 1378, no. 2, pp. F115–77, 1998.

[34] C. Horbinski, M. N. Nikiforova, J. M. Hagenkord, R. L. Hamilton, and I. F. Pollack, "Interplay among braf, p16, p53, and mib1 in pediatric low-grade gliomas," *Neuro-oncology*, vol. 14, no. 6, pp. 777–789, 2012.

[35] E. H. Raabe, K. S. Lim, J. M. Kim, A. Meeker, X.-g. Mao, G. Nikkhah, J. Maciaczyk, U. Kahlert, D. Jain, E. Bar, *et al.*, "Braf activation induces transformation and then senescence in human neural stem cells: a pilocytic astrocytoma model," *Clinical Cancer Research*, vol. 17, no. 11, pp. 3590–3599, 2011.

[36] J. D. Schiffman, J. G. Hodgson, S. R. VandenBerg, P. Flaherty, M.-Y. C. Polley, M. Yu, P. G. Fisher, D. H. Rowitch, J. M. Ford, M. S. Berger, *et al.*, "Oncogenic braf mutation with cdkn2a inactivation is characteristic of a subset of pediatric malignant astrocytomas," *Cancer research*, vol. 70, no. 2, pp. 512–519, 2010.

[37] W.-K. Yun, Y.-M. Hu, C.-B. Zhao, D.-Y. Yu, and J.-B. Tang, "Hcp5 promotes colon cancer development by activating ap1g1 via pi3k/akt pathway.," *European Review for Medical & Pharmacological Sciences*, vol. 23, no. 7, 2019.

[38] J. Shin, A. Nile, and J.-W. Oh, "Role of adaptin protein complexes in intracellular trafficking and their impact on diseases," *Bioengineered*, vol. 12, no. 1, pp. 8259–8278, 2021.

[39] C.-L. Xu, L. Chen, D. Li, F.-T. Chen, M.-L. Sha, and Y. Shao, "Acyl-coa thioesterase 8 and 11 as novel biomarkers for clear cell renal cell carcinoma," *Frontiers in genetics*, vol. 11, p. 594969, 2020.

[40] M. L. Nickerson, E. Jaeger, Y. Shi, J. A. Durocher, S. Mahurkar, D. Zaridze, V. Matveev, V. Janout, H. Kollarova, V. Bencko, *et al.*, "Improved identification of von hippel-lindau gene alterations in clear cell renal tumors," *Clinical cancer research*, vol. 14, no. 15, pp. 4726–4734, 2008.

[41] S. D. Lokeshwar, A. Talukder, T. J. Yates, M. J. Hennig, M. Garcia-Roig, S. S. Lahorewala, N. N. Mullani, Z. Klaassen, B. R. Kava, M. Manoharan, *et al.*, "Molecular characterization of renal cell carcinoma: a potential three-microrna prognostic signature," *Cancer epidemiology, biomarkers & prevention*, vol. 27, no. 4, pp. 464–472, 2018.

[42] X. Liu, L. Zhong, P. Li, and P. Zhao, "microrna-100 enhances autophagy and suppresses migration and invasion of renal cell carcinoma cells via disruption of nox4-dependent mtor pathway," *Clinical and Translational Science*, vol. 15, no. 2, pp. 567–575, 2022.

[43] D. D. Newmeyer and S. Ferguson-Miller, "Mitochondria: releasing power for life and unleashing the machineries of death," *Cell*, vol. 112, no. 4, pp. 481–490, 2003.

[44] T. R. Figueira, M. H. Barros, A. A. Camargo, R. F. Castilho, J. C. Ferreira, A. J. Kowaltowski, F. E. Sluse, N. C. Souza-Pinto, and A. E. Vercesi, "Mitochondria as a source of reactive oxygen and nitrogen species: from molecular mechanisms to human health," *Antioxidants & redox signaling*, vol. 18, no. 16, pp. 2029–2074, 2013.

[45] A. Marquardt, A. G. Solimando, A. Kerscher, M. Bittrich, C. Kalogirou, H. Kübler, A. Rosenwald, R. Bargou, P. Kollmannsberger, B. Schilling, *et al.*, "Subgroup-independent mapping of renal cell carcinoma—machine learning reveals prognostic mitochondrial gene signature beyond histopathologic boundaries," *Frontiers in oncology*, vol. 11, p. 621278, 2021.

[46] J. A. Mayr, D. Meierhofer, F. Zimmermann, R. Feichtinger, C. Kogler, M. Ratschek, N. Schmeller, W. Sperl, and B. Kofler, "Loss of complex i due to mitochondrial dna mutations in renal oncocytoma," *Clinical Cancer Research*, vol. 14, no. 8, pp. 2270–2275, 2008.

[47] S. Joshi, D. Tolkunov, H. Aviv, A. A. Hakimi, M. Yao, J. J. Hsieh, S. Ganesan, C. S. Chan, and E. White, "The genomic landscape of renal oncocytoma identifies a metabolic barrier to tumorigenesis," *Cell reports*, vol. 13, no. 9, pp. 1895–1908, 2015.

[48] M. J. Merino, C. Torres-Cabala, P. Pinto, and W. M. Linehan, "The morphologic spectrum of kidney tumors in hereditary leiomyomatosis and renal cell carcinoma (hlrcc) syndrome," *The American journal of surgical pathology*, vol. 31, no. 10, pp. 1578–1585, 2007.

[49] S. R. Williamson, J. N. Eble, M. B. Amin, N. S. Gupta, S. C. Smith, L. M. Sholl, R. Montironi, M. S. Hirsch, and J. L. Hornick, "Succinate dehydrogenase-deficient renal cell carcinoma: detailed characterization of 11 tumors defining a unique subtype of renal cell carcinoma," *Modern pathology*, vol. 28, no. 1, pp. 80–94, 2015.

[50] I. Bossis and C. A. Stratakis, "Minireview: Prkar1a: normal and abnormal functions," *Endocrinology*, vol. 145, no. 12, pp. 5452–5458, 2004.

[51] S. Wang, Y. Cheng, Y. Zheng, Z. He, W. Chen, W. Zhou, C. Duan, and C. Zhang, "Prkar1a is a functional tumor suppressor inhibiting erk/snail/e-cadherin pathway in lung adenocarcinoma," *Scientific Reports*, vol. 6, no. 1, p. 39630, 2016.

[52] M.-F. Galliano, E. Toulza, H. Gallinaro, N. Jonca, A. Ishida-Yamamoto, G. Serre, and M. Guerrin, "A novel protease inhibitor of the α2-macroglobulin family expressed in the human epidermis," *Journal of Biological Chemistry*, vol. 281, no. 9, pp. 5780–5789, 2006.

[53] L. E. Vissers, M. Bonetti, J. Paardekooper Overman, W. M. Nillesen, S. G. Frints, J. De Ligt, G. Zampino, A. Justino, J. C. Machado, M. Schepens, *et al.*, "Heterozygous germline mutations in a2ml1 are associated with a disorder clinically related to noonan syndrome," *European journal of human genetics*, vol. 23, no. 3, pp. 317–324, 2015.

[54] W. Zhang, Q. Cui, W. Qu, X. Ding, D. Jiang, and H. Liu, "Trim58/cg26157385 methylation is associated with eight prognostic genes in lung squamous cell carcinoma," *Oncology Reports*, vol. 40, no. 1, pp. 206–216, 2018.

[55] M. Y. Zhang, L. Q. Wang, and C. S. Chim, "mir-1250-5p is a novel tumor suppressive intronic mirna hypermethylated in non-hodgkin's lymphoma: novel targets with impact on erk signaling and cell migration," *Cell Communication and Signaling*, vol. 19, no. 1, pp. 1–12, 2021.

[56] B. Yuan, R. Zhang, J. Hu, Z. Liu, C. Yang, T. Zhang, and C. Zhang, "Wdr1 promotes cell growth and migration and contributes to malignant phenotypes of non-small cell lung cancer through adf/cofilin-mediated actin dynamics," *International journal of biological sciences*, vol. 14, no. 9, p. 1067, 2018.

[57] R. P. Young, R. J. Hopkins, T. Christmas, P. N. Black, P. Metcalf, and G. Gamble, "Copd prevalence is increased in lung cancer, independent of age, sex and smoking history," *European Respiratory Journal*, vol. 34, no. 2, pp. 380–386, 2009.

[58] J. Xue, S. Yang, and S. Seng, "Mechanisms of cancer induction by tobacco-specific nnk and nnn," *Cancers*, vol. 6, no. 2, pp. 1138–1156, 2014.

[59] T. Potapova and G. J. Gorbsky, "The consequences of chromosome segregation errors in mitosis and meiosis," *Biology*, vol. 6, no. 1, p. 12, 2017.

[60] J. E. Park, Y. L. Jang, and C.-Y. Jang, "The tobacco carcinogen nnk disturbs mitotic chromosome alignment by interrupting p53 targeting to the centrosome," *Toxicology Letters*, vol. 281, pp. 110–118, 2017.

[61] E. W.-F. Lam, J. J. Brosens, A. R. Gomes, and C.-Y. Koo, "Forkhead box proteins: tuning forks for transcriptional harmony," *Nature Reviews Cancer*, vol. 13, no. 7, pp. 482–495, 2013.

[62] L. Zhang, L. Li, H. Wei, L. Guo, C. Ai, H. Xu, Z. Wu, and Q. Zhou, "Transcriptional factor foxo3 negatively regulates the expression of nm23-h 1 in non-small cell lung cancer," *Thoracic cancer*, vol. 7, no. 1, pp. 9–16, 2016.

[63] L. Zhang, M. Cai, Z. Gong, B. Zhang, Y. Li, L. Guan, X. Hou, Q. Li, G. Liu, Z. Xue, *et al.*, "Geminin facilitates foxo3 deacetylation to promote breast cancer cell metastasis," *The Journal of Clinical Investigation*, vol. 127, no. 6, pp. 2159–2175, 2017.

[64] D. Ni, X. Ma, H.-Z. Li, Y. Gao, X.-T. Li, Y. Zhang, Q. Ai, P. Zhang, E.-L. Song, Q.-B. Huang, *et al.*, "Downregulation of foxo3a promotes tumor metastasis and is associated with metastasis-free survival of patients with clear cell renal cell carcinoma," *Clinical Cancer Research*, vol. 20, no. 7, pp. 1779–1790, 2014.

[65] A. S. Spencer, D. da Silva Dias, M. L. Capelas, F. Pimentel, T. Santos, P. M. Neves, A. Mäkitie, and P. Ravasco, "Managing severe dysgeusia and dysosmia in lung cancer patients: a systematic scoping review," *Frontiers in oncology*, vol. 11, p. 774081, 2021.

[66] A. A. Nolden, L.-D. Hwang, A. Boltong, and D. R. Reed, "Chemosensory changes from cancer treatment and their effects on patients' food behavior: a scoping review," *Nutrients*, vol. 11, no. 10, p. 2285, 2019.

[67] J. Frowen, R. Hughes, and J. Skeat, "The prevalence of patient-reported dysphagia and oral complications in cancer patients," *Supportive Care in Cancer*, vol. 28, pp. 1141–1150, 2020.

[68] X. Yu, P. Zhong, Y. Han, Q. Huang, J. Wang, C. Jia, and Z. Lv, "Key candidate genes associated with brafv600e in papillary thyroid carcinoma on microarray analysis," *Journal of Cellular Physiology*, vol. 234, no. 12, pp. 23369–23378, 2019.

[69] K. Y. Choi, J. H. Kim, I. S. Park, Y. S. Rho, G. H. Kwon, and D. J. Lee, "Predictive gene signatures of nodal metastasis in papillary thyroid carcinoma," *Cancer Biomarkers*, vol. 22, no. 1, pp. 35–42, 2018.

[70] B. Ozer and U. Sezerman, "Analysis of the interplay between methylation and expression reveals its potential role in cancer aetiology," *Functional & integrative genomics*, vol. 17, pp. 53–68, 2017.

[71] Y. Wang, M. Shi, N. Yang, X. Zhou, and L. Xu, "Gpr115 contributes to lung adenocarcinoma metastasis associated with lamc2 and predicts a poor prognosis," *Frontiers in oncology*, vol. 10, p. 577530, 2020.

[72] L. Yi and Y. Yuan, "Microrna-618 modulates cell growth via targeting pi3k/akt pathway in human thyroid carcinomas," *Indian Journal of Cancer*, vol. 52, no. Suppl 3, pp. e186–e189, 2015.

[73] K. Yanagisawa, H. Osada, A. Masuda, M. Kondo, T. Saito, Y. Yatabe, K. Takagi, T. Takahashi, and T. Takahashi, "Induction of apoptosis by smad3 and down-regulation of smad3 expression in response to tgf-β in human normal lung epithelial cells," *Oncogene*, vol. 17, no. 13, pp. 1743–1747, 1998.

[74] P. M.-K. Tang, S. Zhou, X.-M. Meng, Q.-M. Wang, C.-J. Li, G.-Y. Lian, X.-R. Huang, Y.-J. Tang, X.-Y. Guan, B. P.-Y. Yan, *et al.*, "Smad3 promotes cancer progression by inhibiting e4bp4-mediated nk cell development," *Nature communications*, vol. 8, no. 1, p. 14677, 2017.

[75] Y. Wang, H. He, S. Liyanarachchi, L. K. Genutis, W. Li, L. Yu, J. E. Phay, R. Shen, P. Brock, and A. de la Chapelle, "The role of smad3 in the genetic predisposition to papillary thyroid carcinoma," *Genetics in Medicine*, vol. 20, no. 9, pp. 927–935, 2018.

[76] M. Y. Asghar, T. Lassila, and K. Törnquist, "Calcium signaling in the thyroid: Friend and foe," *Cancers*, vol. 13, no. 9, p. 1994, 2021.

[77] I. Salama, P. Malone, F. Mihaimeed, and i. J. Jones, "A review of the s100 proteins in cancer," *European Journal of Surgical Oncology (EJSO)*, vol. 34, no. 4, pp. 357–364, 2008.

[78] J. Zhong, C. Liu, Y.-j. Chen, Q.-h. Zhang, J. Yang, X. Kang, S.-R. Chen, G.-b. Wen, X.-y. Zu, and R.-x. Cao, "The association between s100a13 and hmga1 in the modulation of thyroid cancer proliferation and invasion," *Journal of translational medicine*, vol. 14, no. 1, pp. 1–13, 2016.

[79] W. Jia, X.-J. Gao, Z.-D. Zhang, Z.-X. Yang, and G. Zhang, "S100a4 silencing suppresses proliferation, angiogenesis and invasion of thyroid cancer cells through downregulation of mmp-9 and vegf.," *European Review for Medical & Pharmacological Sciences*, vol. 17, no. 11, 2013.

[80] K. A. Ely, L. A. Bischoff, and V. L. Weiss, "Wnt signaling in thyroid homeostasis and carcinogenesis," *Genes*, vol. 9, no. 4, p. 204, 2018.

[81] A. Sastre-Perona and P. Santisteban, "Wnt-independent role of β-catenin in thyroid cell proliferation and differentiation," *Molecular Endocrinology*, vol. 28, no. 5, pp. 681–695, 2014.

[82] C. Soravia, S. L. Sugg, T. Berk, A. Mitri, H. Cheng, S. Gallinger, Z. Cohen, S. L. Asa, and B. V. Bapat, "Familial adenomatous polyposis-associated thyroid cancer: a clinical, pathological, and molecular genetics study," *The American journal of pathology*, vol. 154, no. 1, pp. 127–135, 1999.

[83] K. Kurihara, S.-I. Shimizu, J.-M. Chong, T. Hishima, N. Funata, H. Kashiwagi, H. Nagai, M. Miyaki, and M. Fukayama, "Nuclear localization of immunoreactive β-catenin is specific to familial adenomatous polyposis in papillary thyroid carcinoma," *Japanese journal of cancer research*, vol. 91, no. 11, pp. 1100–1102, 2000.

[84] F. Furuya, J. A. Hanover, and S.-y. Cheng, "Activation of phosphatidylinositol 3-kinase signaling by a mutant thyroid hormone β receptor," *Proceedings of the National Academy of Sciences*, vol. 103, no. 6, pp. 1780–1785, 2006.

[85] N. Kremenevskaja, R. Von Wasielewski, A. Rao, C. Schöfl, T. Andersson, and G. Brabant, "Wnt-5a has tumor suppressor activity in thyroid carcinoma," *Oncogene*, vol. 24, no. 13, pp. 2144–2154, 2005.

[86] T. Sakaue, R. Zingarelli, W. Khadraoui, U. Saini, J. Wallbillich, M. Anbazhakan, R. Warner, K. D. P. Dorayappan, D. Kalaiyarasan, M. Morton, *et al.*, "Obesity-associated endometrial cancer: Identifying the contributions of tmem205 expression to the pathogenesis of disease," *Cancer Research*, vol. 83, no. 7_Supplement, pp. 4236–4236, 2023.

[87] L. Liu, S. Ito, N. Nishio, Y. Sun, N. Chen, Y. Tanaka, and K.-i. Isobe, "Gadd34 facilitates cell death resulting from proteasome inhibition," *Anticancer research*, vol. 35, no. 10, pp. 5317–5324, 2015.

[88] T. Zhang, Q. Zhang, J. Zhang, R. Zhao, S. Wei, R. Shi, S. Liu, Q. Zhang, and H. Wang, "An effective er stress-related gene signature predicts overall survival and associates with tumor immunity of patients with endometrial cancer," 2023.

[89] E. S. Ratner, D. Tuck, C. Richter, S. Nallur, R. M. Patel, V. Schultz, P. Hui, P. E. Schwartz, T. J. Rutherford, and J. B. Weidhaas, "Microrna signatures differentiate uterine cancer tumor subtypes," *Gynecologic oncology*, vol. 118, no. 3, pp. 251–257, 2010.

[90] S. Huang, L. Sun, P. Hou, K. Liu, and J. Wu, "A comprehensively prognostic and immunological analysis of actin-related protein 2/3 complex subunit 5 in pan-cancer and identification in hepatocellular carcinoma," *Frontiers in Immunology*, vol. 13, p. 944898, 2022.

[91] T. Kinoshita, N. Nohata, H. Watanabe-Takano, H. Yoshino, H. Hidaka, L. Fujimura, M. Fuse, T. Yamasaki, H. Enokida, M. Nakagawa, *et al.*, "Actin-related protein 2/3 complex subunit 5 (arpc5) contributes to cell migration and invasion and is directly regulated by tumor-suppressive microrna-133a in head and neck squamous cell carcinoma," *International journal of oncology*, vol. 40, no. 6, pp. 1770–1778, 2012.

[92] Y. Moriya, N. Nohata, T. Kinoshita, M. Mutallip, T. Okamoto, S. Yoshida, M. Suzuki, I. Yoshino, and N. Seki, "Tumor suppressive microrna-133a regulates novel molecular networks in lung squamous cell carcinoma," *Journal of human genetics*, vol. 57, no. 1, pp. 38–45, 2012.

[93] S. Zhang and X. Han, "The regulatory role of lipid metabolism in endometrial cancer," *Journal of oncology*, vol. 2022, p. 6458877, 2022.

[94] C. Marquis, C. L. Fonseca, K. A. Queen, L. Wood, S. E. Vandal, H. L. Malaby, J. E. Clayton, and J. Stumpff, "Chromosomally unstable tumor cells specifically require kif18a for proliferation," *Nature communications*, vol. 12, no. 1, p. 1213, 2021.

[95] A. Noatynska, M. Gotta, and P. Meraldi, "Mitotic spindle (dis) orientation and disease: cause or consequence?," *Journal of Cell Biology*, vol. 199, no. 7, pp. 1025–1035, 2012.

[96] J. M. Nicholson and D. Cimini, "How mitotic errors contribute to karyotypic diversity in cancer," *Advances in cancer research*, vol. 112, pp. 43–75, 2011.